Journal of Solid State Chemistry 184 (2011) 1551–1555

Contents lists available at ScienceDirect

Journal of Solid State Chemistry

journal homepage: www.elsevier.com/locate/jssc

Enhanced thermal- and photo-stability of acid yellow 17 by incorporation into layered double hydroxides

Qian Wang, Yongjun Feng, Junting Feng, Dianqing Li *

College of Science, State Key Laboratory of Chemical Resource Engineering, Beijing University of Chemical Technology, Beijing 100029, China

ARTICLE INFO

Article history:
Received 29 December 2010
Received in revised form
26 March 2011
Accepted 9 April 2011
Available online 20 April 2011

Keywords:
Dye
Layered double hydroxides
Intercalation
Thermal-stability
Photo-stability
Pigment

ABSTRACT

2,5-dichloro-4-(5-hydroxy-3-methyl-4-(sulphophenylazo) pyrazol-1-yl) benzenesulphonate (DHSB) anions, namely acid yellow 17 anions, have been successfully intercalated into Zn–Al layered double hydroxides (LDH) to produce a novel organic-inorganic pigment by a simple method involving separate nucleation and aging steps (SNAS), and the dye-intercalated LDH was analyzed by various techniques, e.g., XRD, SEM, FT-IR, TG–DTA and ICP. The *d*-spacing of the prepared LDH is 2.09 nm. Furthermore, the incorporation of the DHSB aims to enhance the thermal- and photo-stability of the guest dye molecule, for example, the less color change after accelerated thermal- and photo-aging test.

1. Introduction

Pigments, as one kind of important additives, have been widely used for paints, inks and plastics [1]. According to Ceresana research's report, the worldwide market for inorganic, organic and special pigments had a total volume of ca. 7.4 million tons in 2006 and, furthermore, this volume is expected up to 9.8 million tons in 2016 at an increasing rate of 2.9% per year. Compared with inorganic pigments, organic pigments have brighter color, higher color strength, better transparence and higher chemical stability, but worse light fastness. The worse light fastness of organic pigments mainly results from their poor thermo- and photo-stability. Therefore, it is an important and interesting issue to explore novel pigments with high thermo- and photo-stability as required for practical applications.

Layered double hydroxides (LDH), one class of anionic layered clays, is usually described by a general formula $[M^{2+}_{1-x}M^{3+}_{x}(OH)_2]^{x+}(A^{n-})_{x/n}\cdot mH_2O$ [often abbreviated as $M^{2+}_{y}M^{3+}-A$ LDH, $y=(1-x)/x$, $0.2<x<0.33$], where M^{2+} and M^{3+} are di- and trivalent metal cations in the brucite-like host sheet, and A^{n-} is the guest anions in the interlayer galleries [2,3]. Up to date, a lot of synthesis methods have been developed to prepare LDH materials with different chemical composition in the host sheet and various functional guest anions in the interlayer region, for example, coprecipitation, anion-exchange, hydrothermal and rehydration [2,4]. Usually, the coprecipitation method is used to prepare LDHs containing simple guest anions (e.g., NO_3^-, Cl^-) as the precursor for the anion-exchange method to produce multi-functional LDHs containing complex functional anions [5,6]. On the basis of coprecipitation method, our laboratory has invented a method involving separate nucleation and aging steps (SNAS) to synthesize LDH materials with small particle size and narrow size distribution [7,8]. Compared with others, this method is faster and more facile, particularly more suitable for large batch product. Based on their structure characteristics: adjustable structure, tunable chemical composition and exchangeable interlayer anions, LDH materials have wide applications [9,10] as catalysts [2,11–14], IR absorption materials [15,16], photo functional materials [17–19], flame retardants [20], etc. Thus, it is possible to intercalate coloring dye anions into the interlayer galleries of LDHs to produce novel organic-inorganic composite pigments. These pigments may have brilliant color like organic pigments and relatively high thermo- and photo-stability thanks to the protection by the LDH host sheet.

A few of organic coloring agents (dyes and pigments) have been intercalated into the interlayer galleries of LDH materials, for example, acid blue 9 [21], methyl orange [22], blue dye molecules [23] and chromophore molecules [24]. Most of them have mainly investigated the assembling methods of anions and the corresponding structure. Few researchers, however, have paid special attention to the influence of the LDH structure on the tolerance of the organic anions towards thermal and photo aging

* Corresponding author. Fax: +86 10 6442 5385.
E-mail addresses: lidq@mail.buct.edu.cn, dianqingli@163.com (D. Li).

0022-4596/$ - see front matter © 2011 Elsevier Inc. All rights reserved.
doi:10.1016/j.jssc.2011.04.020

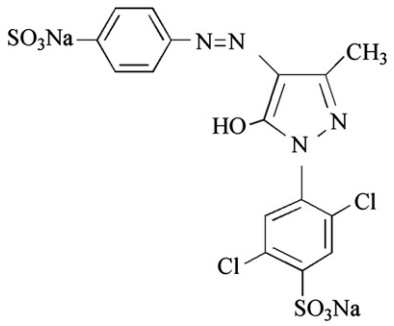

Fig. 1. Chemical structural formula of DDHSB.

[24]. In our group, we have intercalated some pigment and dye guest molecules (e.g., Red 48:2 [25], Red 52:1 [26], Mordant Yellow MY10 [27]) into the LDH materials and found that the LDH structure favors improvement of the thermal and photo-stability.

Disodium 2, 5-dichloro-4-(5-hydroxy-3-methyl-4-(sulphophenylazo)pyrazol-1-yl) benzenesulphonate (abbreviated as DDHSB), namely acid yellow 17, one of three basic color dyes, is widely used for textile, paper, paint, medicine and cosmetic, see its chemical structural formula in Fig. 1. In this work, we mainly investigated the direct preparation of the DHSB intercalated LDH by the SNAS method and the corresponding thermal and photo-stability by accelerated aging techniques.

2. Material and methods

2.1. Material

All the chemicals, except for DDHSB, were A.R grade and used as received from Beijing Yili Fine Chemical Reagent Co. without any further purification. DDHSB (98 wt%) was recrystallized three times in water before use. Deionized water with conductivity less than 10^{-6} S cm^{-1} was freshly decarbonated by boiling before use in all of the synthesis and washing steps.

2.2. Preparation of ZnAl-DHSB-LDH

ZnAl-DHSB-LDH was directly synthesized by the SNSA method [7,8]. Typically, $Zn(NO_3)_2 \cdot 6H_2O$ (11.90 g, 0.04 mol), $Al(NO_3)_3 \cdot 9H_2O$ (7.50 g, 0.02 mol) and DDHSB (8.26 g, 0.015 mol) were dissolved in CO_2-free deionized water to make a mixed salt solution A (100 mL); NaOH (4.80 g, 0.12 mol) was dissolved in CO_2-free deionized water to form an alkali solution B (100 mL). Solutions A and B were simultaneously and slowly added into a colloid mill at a rotor speed of 3000 rpm and mixed for another 2 min. Then, the resulting slurry was aged at the refluxing temperature (102 °C) for 8 h under a N_2 stream. The final product was collected by centrifuging (4200 rpm for 5 min each time), washing with water, ethylene glycol and N,N-dimethylformamide until the solution without color, and drying at 80 °C to constant weight.

2.3. Analysis and characterization

Powder X-ray diffraction (XRD) measurements were performed on Shimadzu XRD-6000 X-ray powder diffractometer (Cu $K\alpha$ radiation, $\lambda = 0.154$ nm) from 3° to 70° with a steplength of 0.02° at a scanning rate of 0.02° s^{-1}. High-resolution transmission electron microscopy (HRTEM) was carried out on a JEOL JEM-2100 microscope operated at 200 kV (point resolution, 0.19 nm and line resolution, 0.14 nm). FT-IR spectra were recorded on a Bruker Vector 22 Fourier transfer infrared spectrophotometer using the KBr pellet method with a ratio of sample/KBr of 1:100 by weight. Thermogravimetry and differential thermal analysis (TG–DTA) curves were obtained on a PCT-IA instrument in the range of 30–700 °C at a rate of 10 °C min^{-1} under air. Diffuse reflectance UV–vis absorbance spectra were collected on Shimadzu UV-2501PC with an integrating sphere attachment in the range of 200–800 nm using $BaSO_4$ as the reference. Elemental analysis was carried out on a Shimadzu ICPS-7500 inductively coupled plasma (ICP) emission spectrometer using concentrated nitric acid (65 wt%) as the dissolving agent. The color difference (ΔE) of materials after thermal- and photo-aging treatment was determined in terms of CIE 1976 $L^*a^*b^*$ with a TC-P2A automatic colorimeter [25].

3. Results and discussion

3.1. Structure and morphology of ZnAl-DHSB-LDH

Fig. 2 displays XRD patterns of ZnAl-DHSB-LDH. Here, the first three Bragg reflection peaks locate at 4.22° (2.09 nm), 8.45° (1.05 nm) and 12.66° (0.70 nm)/2-theta (d-value), respectively. One may note a simple multiple between these three d-values, for example, $2.09\ \text{nm} \approx 2 \times 1.05\ \text{nm} \approx 3 \times 0.70\ \text{nm}$ showing a typically layered structure like the LDH [2]. It is worthy to note no XRD pattern for ZnAl-NO_3-LDH, indicating that the SNSA method is available for direct preparation of the LDH materials containing relatively complex anions besides simple anions, e.g., CO_3^{2-} [7,8] and NO_3^- [15]. The cell parameters are estimated based on structural features of LDH materials: $a = 2d_{110} = 0.303$ nm and $c = 3d_{003} = 6.27$ nm. Here, remind that both of 110 and 113 Bragg reflections are usually overlapped for the intercalated LDHs as observed in ref. [28,29]. We separate the broad peak from 60° to 62.7°/2θ to two peaks using Gauss function: 60.76°/2θ for 110 and 61.57°/2θ for 113, see the inset graph in Fig. 2. The calculated a value is in agreement with those reported in the literature for Zn_2Al LDH [28] since the a value mainly depends on the composition of the brucite-like host sheet.

Besides, Fig. 3 shows the HRTEM micrographs of the intercalated LDH. One observes the average particle size ca. 50 nm with narrow size distribution. Moreover, the basal spacing of ZnAl-DHSB LDH is detected from the average distance between the parallel fringes as marked in Fig. 3B and C. The evaluated value of ca. 2.25 nm (11.26 nm/5) is in good agreement with the d_{003} value of 2.09 nm determined by XRD.

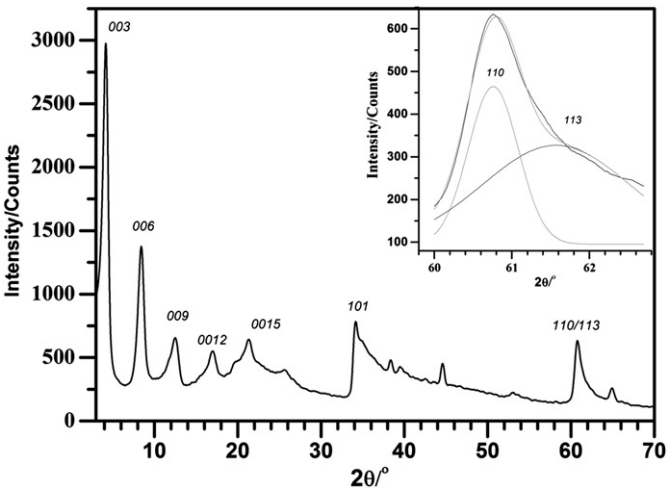

Fig. 2. Powder X-ray diffraction (XRD) patterns of ZnAl-DHSB-LDH.

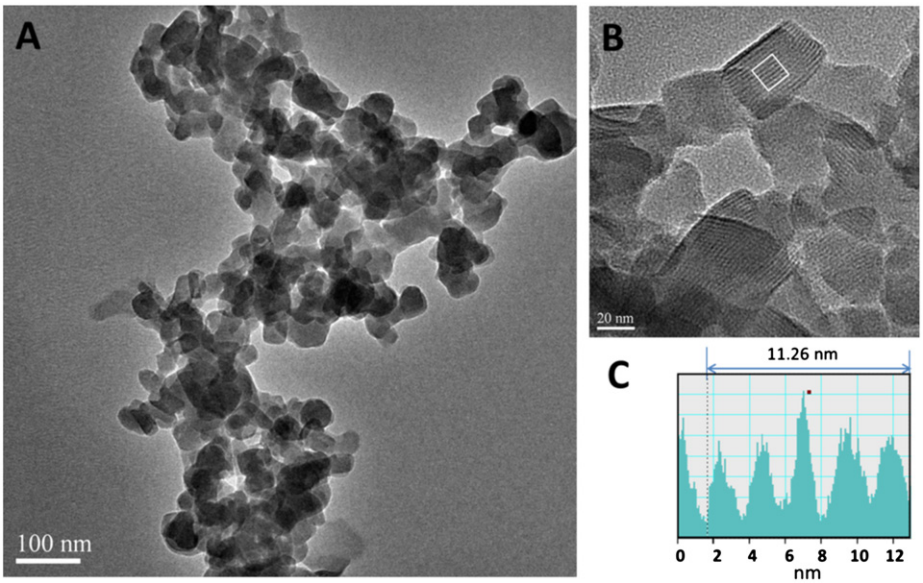

Fig. 3. HRTEM observation of ZnAl-DHSB-LDH: (A) low magnification with a scale bar of 100 nm, (B) high magnification with a scale bar of 20 nm, and (C) intensity histogram of the area marked in part B.

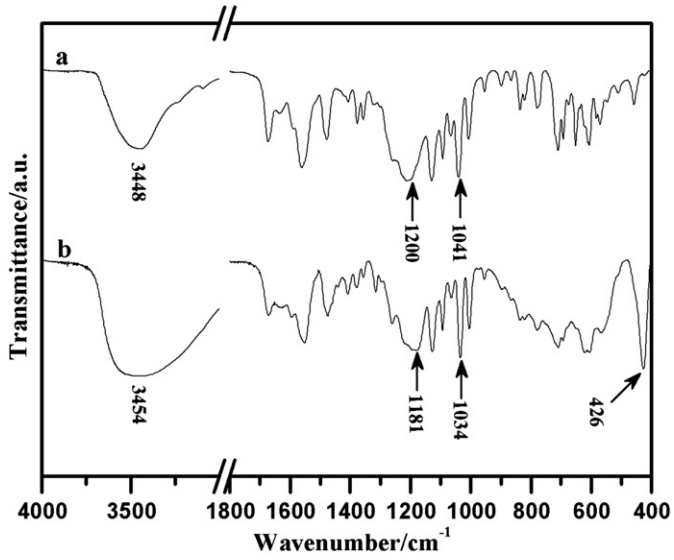

Fig. 4. FT-IR spectra of (a) DDHSB and (b) ZnAl-DHSB-LDH. The position of some characteristic absorption bands are marked in the graph.

3.2. FT-IR analysis of ZnAl-DHSB-LDH

Fig. 4 illustrates the FT-IR spectra of DDHSB molecule and ZnAl-DHSB-LDH. In Fig. 4a, the absorption band at ca. 3448 cm^{-1} is assigned to the hydroxyl groups stretching vibration of adsorbed water. Both absorption bands centered at 1200 and 1041 cm^{-1} are attributed to the asymmetric and symmetric stretching vibrations of the $-SO_3^-$ group, respectively. In Fig. 4b, the broad band at ca. 3454 cm^{-1} is due to the O–H stretching vibration in the brucite-like layers, which locates at much lower frequency related to that at 3600 cm^{-1} in free water [30]. This result may result from the influence of hydrogen bonding between interlayer water and hydroxyl groups of the host layers [31]. The characteristic absorption bands for $-SO_3^-$ group shift to lower frequency at 1181 and 1034 cm^{-1}, indicating the existence of strong interaction between the host layers and the guest anions. Besides the IR spectra of the guest anions, the absorption band in the range from 400 to 800 cm^{-1} is ascribed to O–M–O vibrations in the brucite-like layers of the LDH [29]. Here, it is worth mentioning that the strong band for nitrate anions at 1380 cm^{-1} is absent [32], which is in agreement with the results of XRD.

3.3. TG–DTA analysis

Fig. 5 demonstrates TG–DTA curves of DDHSB and ZnAl-DHSB-LDH. In Fig. 5a, four weight-loss stages in the TG curve are observed: 30–180, 180–294, 294–425 and 425–700 °C, which correspond to two endothermic peaks (134 and 226 °C) and two exothermic peaks (370 and 487 °C) in the DTA curve, respectively. The first stage can be attributed to the release of the physical adsorption water; the second stage results from the partial release of chemical adsorption water; the third one is possibly caused due to the oxidation of the DDHSB; the fourth one is related to combustion of the molecule fragment.

Compared with Fig. 5a, b shows three weight-loss stages in the TG curve at ca. 100–230, 230–300 and 300–700 °C, which are attributed to the release of interlayer water, dehydroxylation in the brucite-like sheet [2,14] and the combustion of the interlayer organic anions, respectively. Three weight-loss stages correspond to two endothermic peaks centered at 173 and 268 °C, and one exothermic peak at ca. 508 °C.

3.4. Chemical composition of ZnAl-DHSB-LDH

The weight percent of the individual element in the composition was examined by ICP and the results are 23.56 wt% for Zn, 4.82 wt% for Al and 5.88 wt% for S. According to the general formula of the LDH, the formula of the prepared product is obtained as $[Zn_{0.67}Al_{0.33}(OH)_2](DHSB)_{0.17}\cdot 0.76H_2O$. The water content (ca. 7.41 wt%) in the formula is calculated from TG data in the range 100–230 °C, see Fig. 5b.

3.5. Model of supramolecular intercalation structure

The results of XRD patterns (Fig. 2) and FT-IR spectra (Fig. 4) suggest that ZnAl-DHSB-LDH has a typical pillared structure and supramolecular interaction. The *d*-spacing of 2.09 nm is smaller

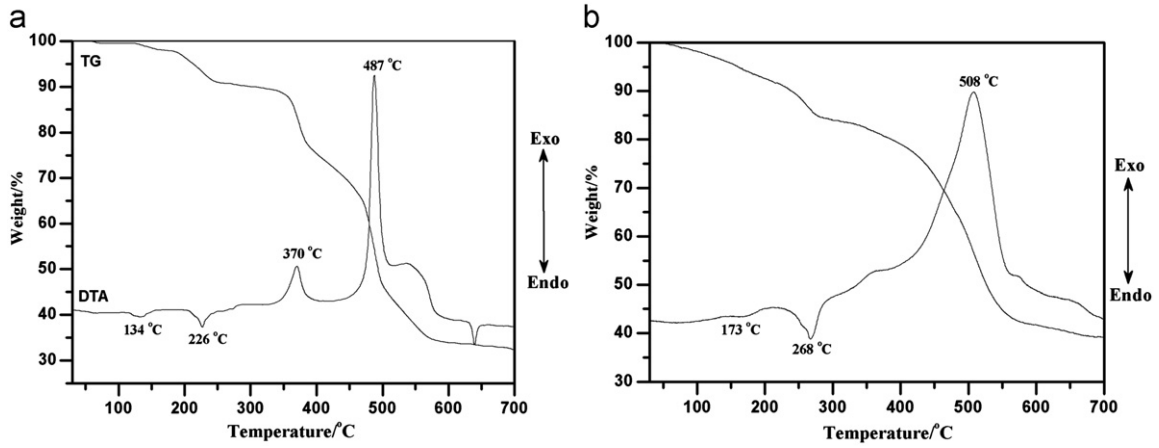

Fig. 5. TG–DTA curves of (a) DDHSB and (b) ZnAl-DHSB-LDH recorded from 30 to 700 °C at a rate of 10 °C min^{-1} under air.

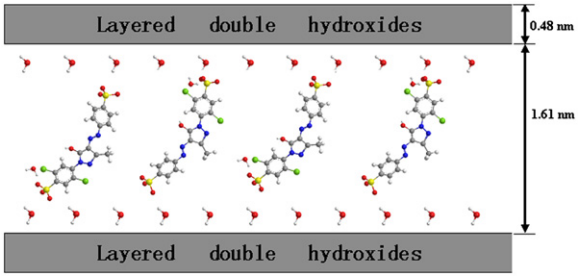

Fig. 6. Supramolecular structural model of ZnAl-DHSB-LDH.

than the sum of the thickness of the brucite-like layer (ca. 0.48 nm [33]) plus the length of the DHSB anion in the longest direction (ca. 2.21 nm). Therefore, the interlayer DHSB anions are probably arranged as a monolayer, with tilted orientation with respect to the hydroxide layers, as shown in Fig. 6.

3.6. Thermostability and photo-stability analysis of DDHSB and ZnAl-DHSB-LDH

The thermostability of DDHSB and ZnAl-DHSB-LDH was investigated at different temperature in the range from 100 to 300 °C for 30 min. Each heated sample was measured by diffuse reflectance UV–vis spectroscopy and automatic colorimeter. Fig. 7 shows diffuse reflectance UV–vis spectra of two samples heated at five different temperatures. On heated below 200 °C, both samples have no change. When the heating temperature is beyond 200 °C, both of them have change to some different extent. However, the intercalated LDH has relatively less change than the guest molecule. The same trend is also observed in Fig. 8. The color difference (ΔE) value for the DDHBS is obviously larger than that for ZnAl-DHBS-LDH, for example, the ΔE of 11 for the DDHSB and that of 6 for the intercalated LDH. Both results show that the intercalation of DHSB into LDH favors to improve thermostability of the DDHSB, possibly due to the strong interaction between the host sheet and the guest anions.

The photo-stability properties of DDHSB and ZnAl-DHSB-LDH were investigated at 70 °C using a UV accelerated photo-aging instrument (power of the UV light = 1000 W and λ_{max} = 365 nm) with a controllable temperature system as described elsewhere [17]. The sample was exposed to UV lamp for 5 min and then the color change was recorded by automatic colorimeter. The same process was repeated for 10 times and then the accumulated

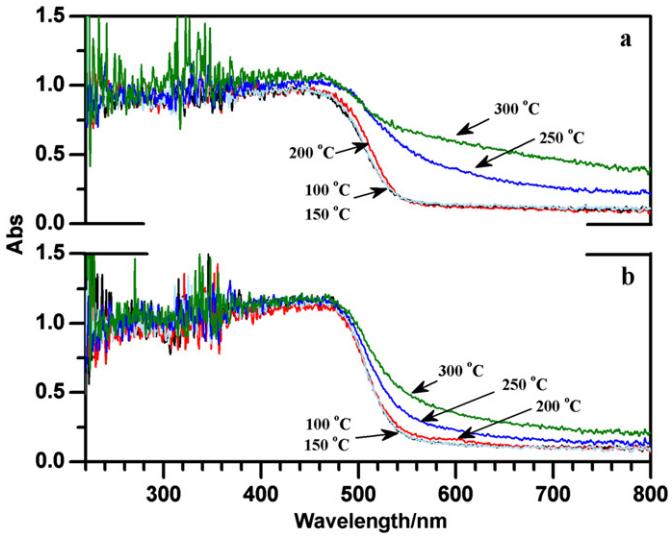

Fig. 7. Diffuse reflectance UV–vis spectra of (a) DDHSB and (b) ZnAl-DHSB-LDH collected after heated at 100, 150, 200, 250 and 300 °C for 30 min.

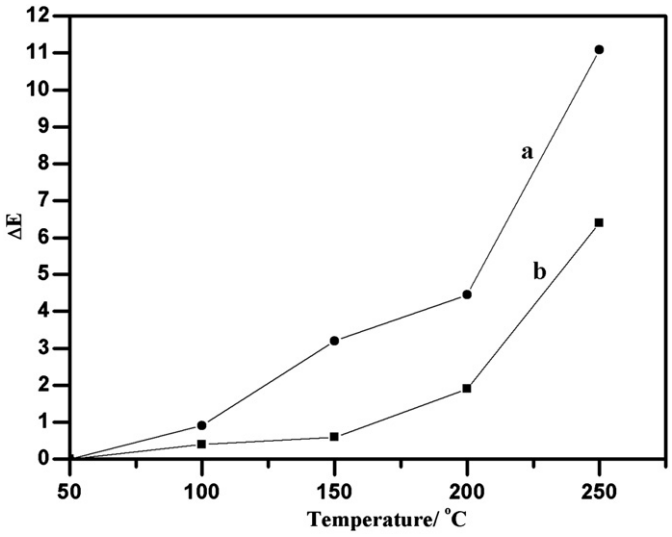

Fig. 8. Color difference (ΔE) values of (a) DDHSB and (b) ZnAl-DHSB-LDH after heated at 100, 150, 200 and 250 °C for 30 min.

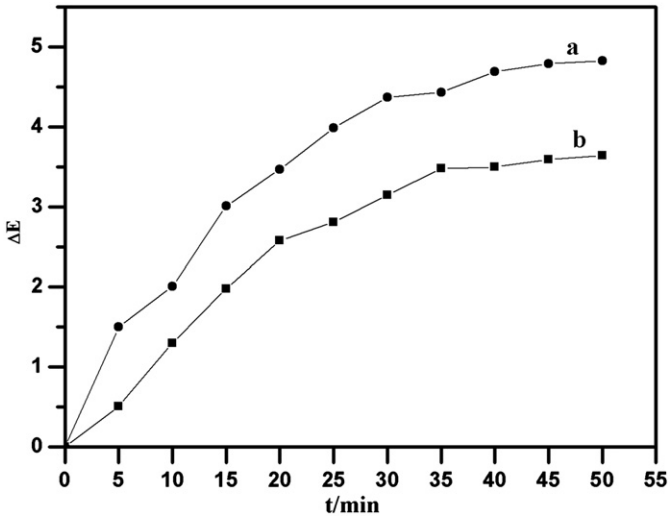

Fig. 9. Color difference (ΔE) values of (a) DDHSB and (b) ZnAl-DHSB-LDH after photo aging from 5 to 50 min.

photo-aging time is 50 min. As shown in Fig. 9, the ΔE value of DDHSB is obviously larger than that of ZnAl-DHSB-LDH for the same aging time, and the different value between the ΔE values of two samples is increasing as the irradiation time prolonged. The results demonstrate that the ZnAl-DHSB-LDH has higher photo-stability than DDHSB under the investigated conditions.

4. Conclusions

The dye-intercalated LDH has been successfully and directly prepared to produce organic-inorganic composite pigment by the method involving separate nucleation and aging steps. Compared with the guest dye molecule, the dye-intercalated LDH has higher thermal- and photo-stability under the investigated conditions, possibly thanks to the strong interaction between the host sheet and the guest anions. Other dye molecules with poor thermal- and photo-stability may be intercalated into the galleries of LDH materials to enhance their stability and then extend their applications in different fields.

Acknowledgment

This work was supported by the National Natural Science Foundation of China (Nos. 20971013 and 21036001).

References

[1] G. Buxbaum, G. Pfaff, Industrial Inorganic Pigments, 3rd ed., Wiley-VCH, Weinheim, 2005.
[2] F. Cavani, F. Trifirò, A. Vaccari, Catal. Today 11 (1991) 173–301.
[3] D.G. Evans, R.C. Slade, Struct. Bonding 119 (2006) 1–87.
[4] J. He, M. Wei, B. Li, Y. Kang, D.G. Evans, X. Duan, Struct. Bonding 119 (2006) 89–119.
[5] C. Taviot-Guého, Y.J. Feng, A. Faour, F. Leroux, Dalton Trans. 39 (2010) 5994–6005.
[6] A.I. Khan, G.R. Williams, G. Hu, N.H. Rees, D. O'Hare, J. Solid State Chem. 183 (2010) 2877–2885.
[7] Y. Zhao, F. Li, R. Zhang, D.G. Evans, X. Duan, Chem. Mater. 14 (2002) 4286–4291.
[8] Y.J. Feng, D.Q. Li, C.X. Li, Z.H. Wang, D.G. Evans, X. Duan, Clays Clay Miner. 51 (2003) 566–569.
[9] C.-H. Zhou, Appl. Clay Sci. 48 (2010) 1–4.
[10] F. Li, X. Duan, Struct. Bonding 119 (2006) 193–223.
[11] V. Rives, M.Angeles Ulibarri, Coord. Chem. Rev. 181 (1999) 61–120.
[12] M.-Q. Zhao, Q. Zhang, J.-Q. Huang, J.-Q. Nie, F. Wei, Carbon 48 (2010) 3260–3270.
[13] D.S. Tong, C.H. Zhou, M.Y. Li, W.H. Yu, J. Beltramini, C.X. Lin, Z.P. Xu, Appl. Clay Sci. 48 (2010) 569–574.
[14] W. Kagunya, Z. Hassan, W. Jones, Inorg. Chem. 35 (1996) 5970–5974.
[15] L.J. Wang, X.Y. Xu, D.G. Evans, X. Duan, D.Q. Li, J. Solid State Chem. 183 (2010) 1114–1119.
[16] L.J. Wang, X.Y. Xu, D.G. Evans, D.Q. Li, Ind. Eng. Chem. Res. 49 (2010) 5339–5346.
[17] Y.J. Feng, D.Q. Li, Y. Wang, D.G. Evans, X. Duan, Polym. Degrad. Stab. 91 (2006) 789–794.
[18] T. Tanaka, S. Nishimoto, Y. Kameshima, J. Matsukawa, Y. Fujita, Y. Takaguchi, M. Matsuda, M. Miyake, J. Solid State Chem. 183 (2010) 479–484.
[19] W. Shi, M. Wei, D.G. Evans, X. Duan, J. Mater. Chem. 20 (2010) 3901–3909.
[20] D.-Y. Wang, A. Das, F.R. Costa, A. Leuteritz, Y.-Z. Wang, U. Wagenknecht, G. Heinrich, Langmuir 26 (2010) 14162–14169.
[21] A.R. Auxilio, P.C. Andrews, P.C. Junk, L. Spiccia, D. Neumann, W. Raverty, N. Vanderhoek, Polyhedron 26 (2007) 3479–3490.
[22] H. Laguna, S. Loera, I.A. Ibarra, E. Lima, M.A. Vera, V. Lara, Microporous Mesoporous Mater. 98 (2007) 234–241.
[23] R. Marangoni, C. Taviot-Guého, A. Illaik, F. Wypych, F. Leroux, J. Colloid Interface Sci. 326 (2008) 366–373.
[24] J. Bauer, P. Behrens, M. Speckbacher, H. Langhals, Adv. Funct. Mater. 13 (2003) 241–248.
[25] S. Guo, D. Li, W. Zhang, M. Pu, D.G. Evans, X. Duan, J. Solid State Chem. 177 (2004) 4597–4604.
[26] S. Guo, D.G. Evans, D. Li, J. Phys. Chem. Solids 67 (2006) 1002–1006.
[27] M. Pu, Y.-H. Liu, L.-Y. Liu, X.-Z. Dong, J. He, D.G. Evans, J. Phys. Chem. Solids 69 (2008) 1084–1087.
[28] E. Káfuňková, C. Taviot-Guého, P. Bezdička, M. Klementová, P. Kovář, P. Kubát, J.i. Mosinger, M. Pospíšil, K. Lang, Chem. Mater. 22 (2010) 2481–2490.
[29] Z.P. Xu, H.C. Zeng, Chem. Mater. 13 (2001) 4555–4563.
[30] K. Nakamoto, Infrared and Raman Spectra of Inorganic and Coordination Compounds, fourth ed., Wiley, New York, 1986.
[31] J.T. Kloprogge, R.L. Frost, J. Solid State Chem. 146 (1999) 506–515.
[32] J.T. Kloprogge, D. Wharton, L. Hickey, R.L. Frost, Am. Mineral. 87 (2002) 623–629.
[33] M. Meyn, K. Beneke, G. Lagaly, Inorg. Chem. 29 (1990) 5201–5207.